6th ECCOMAS Thematic Conference on the Mechanical Response of Composites
COMPOSITES 2017
J.J.C. Remmers and A. Turon (Editors)

PERIDYNAMICS: CONVERGENCE & INFLUENCE OF PROBABILISTIC MATERIAL DISTRIBUTION ON CRACK INITIATION

Martin Rädel[⋆], Anna-Janina Bednarek[⋆], Jochen Schmidt[†], Christian Willberg[⋆]

[⋆]Structural Mechanics Department
[†]Composite Technology Department
Institute for Composite Structures and Adaptive Systems, German Aerospace Center (DLR)
Lilienthalplatz 7, D-38108 Braunschweig, Germany
christian.willberg@dlr.de

Keywords: Peridynamics, Fracture, Mesh dependence.

Summary: *Simulations based on the peridynamic theory are a promising approach to understand the processes involved in matrix failure inside fibre reinforced plastics. Before such complex simulations are carried out, the material behavior of bulk resin material as well as the influence of numerical parameters have to be investigated. In the present text, the linear elastic part of the material response is used to examine the convergence behavior of peridynamic simulations. Possibilities to minimize the effect of different discretization schemes are explored by means of a stochastic material distribution in correlation with scatter found in the material tests regarding the elastic material response and failure patterns. This procedure may also be used to investigate the nature of failure initiation and the robustness of the solution.*

δ	horizon	ρ	mass density	θ	dilatation
$\boldsymbol{\epsilon}$	strain tensor	$\boldsymbol{\sigma}$	Cauchy stress tensor	G	shear modulus
$\mathcal{H}$	neighborhood	K	bulk modulus	V	volume
V_w	weighted volume	$\underline{\omega}$	influence function	$\underline{t}$	pairwise force density
$\underline{x}$	initial bond length	$\underline{y}$	deformed bond length	$\underline{e}$	bond extension
$\mathbf{b}$	external forces	$\mathbf{u}$	displacements	$\ddot{\mathbf{u}}$	acceleration
$\mathbf{x}$	initial position of reference point	$\mathbf{x}'$	initial position of family point	$\mathbf{y}$	deformed position of reference point
$\mathbf{y}'$	deformed position of family point	$\underline{\mathbf{T}}$	force vector state	$\underline{\mathbf{Y}}$	peridynamic state

1. INTRODUCTION & LITERATURE

1.1 Motivation

Today, the full exploitation of the lightweight potential of fibre reinforced plastics (FRP) is limited due to missing reliability of failure predictions of real structures, especially when taking

into account determining manufacturing conditions. The underlying goal behind this study is to increase the understanding of failure mechanisms in FRP as shown in Figure 1 and their numerical simulation.

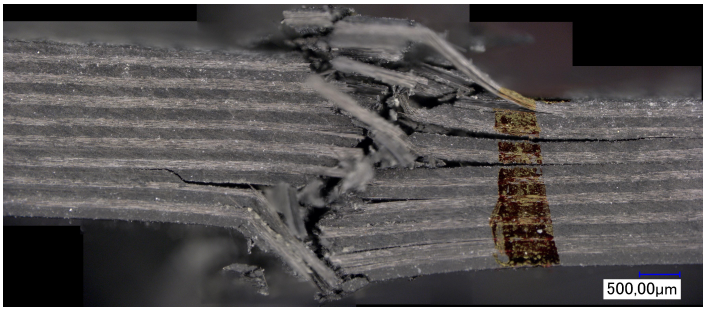

(a) Crack in a CFRP specimen. Courtesy of DLR.

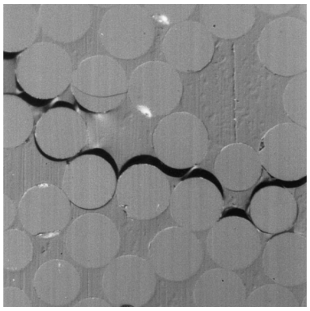

(b) Matrix failure [1, 2]

Figure 1: Exemplary failure mechanisms in FRP materials

The current state-of-the-art methods used in industry and research for failure predictions are based on continuum mechanics (CM) and its numerical implementation in the finite element method (FEM). The continuum mechanics is well suited for stress analyses of undamaged structures, but it is unable to proper model damage evolution after initiation. The basic continuum mechanical theory was originally developed around 1822 by Augustin-Louis Cauchy [3]. The assumptions made by Cauchy lead to a mathematical description of continuous media partial differential equations (PDE). With proper restrictions, the PDEs are elliptic in equilibrium problems. It is to be noted that the underlying boundary value problems are generally well-posed for typical materials [3]. This made the PDEs solvable even in the pre-computer time. In reality, all materials are discontinuous and heterogeneous. For several problems, the usual assumption that at macroscopic length scales a material can be well approximated as continuous, is not valid. Obviously, a fracture in any material fails to satisfy the smoothness requirement.

To overcome this deficit, additional theories such as fracture mechanics are required and applied. However, certain levels of inconsistencies within the mathematical assumptions between continuum and fracture mechanics still lead to inaccurate damage prediction. Motivated by ideas of molecular dynamics, Stewart Silling developed the fundamental peridynamic theory in the early 2000's as an alternative theory to state-of-the-art modelling approaches [4]. In this theory the fundamental PDE of the momentum conservation is replaced by an integral equation.

Peridynamics (PD) presents a promising approach to simulate damage initiation, evolution and interaction in any material in one holistic approach. It is a non-local theory which takes long-range forces between material points in a certain neighborhood, the horizon δ, into account. Constitutive models in peridynamics depend on finite deformation vectors, as opposed to classical constitutive models which depend on deformation gradients [5]. In contrast to the FEM based on continuum mechanics, the peridynamic governing equations are based on integral equations, which are valid everywhere - whether a discontinuity exists in the material or not. Damage is directly incorporated in the material response.

1.2 Horizon and convergence

A main question in PD simulations is the proper choice of the horizon δ and convergence based on the chosen discretization h, cf. Figure 2. In its basic paper on the meaning of the horizon explains that the value may be viewed as an effective interaction distance for non-local effects [6]. The PD horizon does not have to be constant over the domain. [7] reports that if peridynamics is used to model atomic-scale phenomena, the horizon becomes the cut-off radius of the atomic potential. In the present text an ideally continuous and homogeneous structure is considered, in which the standard local theory applies perfectly until failure. However, we still wish to use peridynamics as a way to model damage and fracture. In this scenario the physics of the interactions between material points do not directly determine the choice of discretization type, size and horizon. [8] found that the two dominant physical mechanisms that lead to size dependency of elastic behavior at the nanoscale are surface energy effects and nonlocal interactions. They estimated the length scales at which the classical model of elasticity breaks down for some real materials. They report that in many materials, the length scale, relevant to forces that determine the bulk properties of materials, far exceeds the interatomic spacing and thus long-range forces contribute to the material behavior. This is particularly true for heterogeneous materials. However, the length scales of interest are still dimensions smaller than the macroscopic behavior investigated in the current context. Thus the question arises: Do discretization, element size and horizon have any influence on the macroscopic failure of the considered structures.

It has been shown in various publications that the classical continuum mechanics is a subset of peridynamics and that for a horizon striving to zero, the peridynamic theory converges to the local solution of continuum mechanics. According to [6] this is since wave dispersion due to the size of the nonlocality is reduced as the horizon decreases. [9] shows the convergence to the local solution for bond-based peridynamics, [10] for an isotropic linear elastic material and [11] show that the state-based, nonlocal peridynamic stress tensor reduces to the classical local Piola-Kirchhoff stress tensor in the limit of a shrinking horizon.

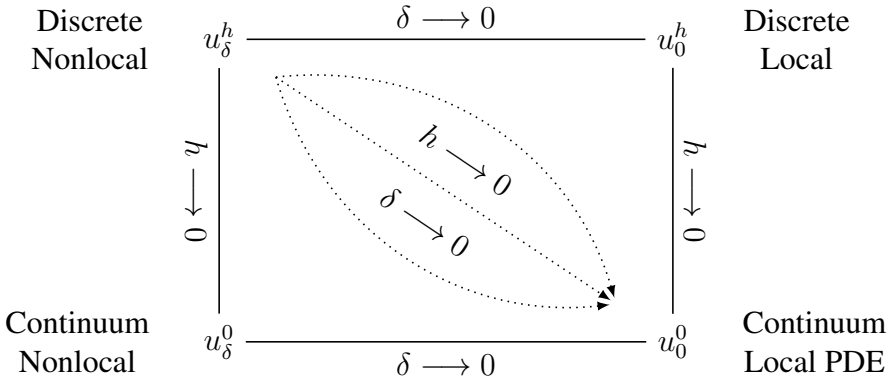

Figure 2: Types of convergence in the peridynamic theory [3]

The convergence of the discretized implementation is a more complex topic compared to the

finite element method due to the two independent parameters of element size dx and horizon δ. In [7, 12] the terms δ- and m-convergence were introduced, where $m = \frac{\delta}{dx}$ for uniformly discretized grids. [13] also discusses these types of convergence.

Therein it is said that δ-convergence is achieved by fixing m while allowing the horizon $\delta \to 0$ or increasing m at a slower rate than the decrease in δ. In [14] δ-convergence is described that if the m-ratio is kept constant, the solution does not change significantly as the horizon tends to zero. For this type of convergence the numerical peridynamic solution converges to an approximate classical solution. The larger the value of m is, in other words the smaller the grid spacing dx is, the better the approximation becomes. However, this convergence may not occur in the presence of discontinuities. A non-continuous convergence behavior is expected for the variation of the two factors. [12] points out that convergence is dependent on the computation scheme of nodal amount of volume of all points in horizon of single point. Its calculation is not easy to perform for nodes that are not entirely contained inside the horizon. Simple algorithms lead to non-uniform m-convergence. The proper choice of horizon has to capture the damage types and the main features of the damage evolution processes and should by performed by means of an absolute length scale, independent of the discretization size [14, 15]. A similar observation was found in [16]. The authors tell that δ should be at least as large as the crack tip plastic process zone, to adequately capture the crack tip physics. Additionally, some experimental intuition may be required to estimate the size of δ if local measurements are not available.

Multiple specific horizon values are suggested in different publications over the years. $\delta \approx 3dx$ and thus $m \approx 3$, especially $m \approx 3.015$, is the most common value and is used for example in [7, 17], [18, 19] for micro brittle material, for bond-based composite DCB and ENF specimen [20] and for a finite element representation of peridynamics via truss elements [21]. In a convergence study [22] found $m \approx 3$ for tension and additionally $m \approx \sqrt{2}$ for compression specimen to be suitable. It has been found that $m \approx 3$ also works well for fracture predictions [17, 23]. $m = 4$ is applied in [6, 24] for dynamic crack branching problems in isotropic materials and in [25] for flow through porous medium. Even larger values are used in [15] for anisotropic materials with $m = 5$ and $m = 6$ in [14] for linear elastic isotropic material. On the other extreme [26] apply $\delta \approx 1.1dx$ for elastic deformation of thin plate in 2D.

Naturally, the necessity for problem-dependent convergence studies becomes obvious. Examples can be found in [27] for a pitting corrosion problem. [28] focused on the convergence of numerical solutions of static PD problems to the analytical solutions of those problems under grid refinement for uniform grids, while keeping the horizon fixed. The source achieves first-order convergence for smooth solutions. Higher convergence rates can be achieved through higher-order discretizations, quadrature-based finite difference discretizations with piecewise linear basis functions [29] or piecewise linear finite element discretizations [29–31], which leads to a second-order convergence of numerical solutions in PD problems characterized by smooth solutions. These higher-order methods, however, significantly increase the complexity of numerical implementations as well as the computational cost of simulations, especially in higher dimensions. [28] found that achieving convergence is challenging, in particular with

respect to the proper choice of horizon. The authors found that, especially in higher dimensions, the horizon cannot be so small as to make computations intractable, but it cannot be too large either as this results in the boundary layer, where displacement boundary conditions are imposed, being the majority of the simulation domain. [32] performs convergence studies for a linear elastic static implementation of non-ordinary state-based PD by means of a zero-energy control term. For δm- & δ-convergence the authors find, the optimum value increases with increasing mesh size, where the magnitude of the control term increases roughly linearly with the number of degrees of freedom. The δm-behavior shows first-order convergence independent of the horizon size, whereas the δ-convergence shows approximately half the rate of convergence. Similar findings are reported by [19]. Therein it is stated that choice of the horizon influences heavily the results. The nodal spacing has to shrink faster than the horizon to obtain convergence. Their results suggest that a good nodal spacing can be found for almost all materials for each horizon and vice versa if a small error is acceptable. Unfortunately, no regular pattern was found from which one can determine a simple functional relation between the horizon and the nodal spacing, which makes the choice of a suitable horizon for a given nodal spacing hard. Somewhat contradictive observations are made in [14]. Therein, the error in 2D linear elasticity state-based PD simulations in which the displacement field is linear is not influenced by δ.

A further question is how to discretize numerical implementations in peridynamics. A simple particle-based discretization for the strong form of peridynamic equations was introduced in [17] and is implemented in currently known codes such as EMU and Peridigm. However, [33] point out that the governing equations in peridynamics are continuum models and can be discretized in many ways. In [28] it is mentioned that commonly used meshfree methods in peridynamics suffer from accuracy and convergence issues, due to a rough approximation of the contribution to the internal force density of nodes near the boundary of the neighborhood of a given node. However they are numerically efficient since finite element discretizations of governing equations are based on weak forms, which for peridynamic equations double the number of spatial dimensions that need to be discretized [30].

Approximately uniform element sizes are used in most publications. PD in Peridigm does allow for small gradients in element size if the horizon definition is modified appropriately in the block definition. [23] proposes an adaptive refinement algorithm for the non-local method 1D bond-based peridynamics. [34] argues that even if convergence is achieved for an element size, when the discretization grid is refined while using the same horizon, the PD solution may start to depart from the classical one, converging to something other than the classical solution.

2. PERIDYNAMICS

PD is a non-local theory to describe the physics of materials. Several assumptions made by the classical continuum mechanics theory are weakened or omitted. In continuum mechanics the medium has to be continuous, the internal forces are contact forces and interact in zero distance to each other. The deformation has to be two times differentiable [3]. These assumptions have no physical motivation. In [35] the comparison of the continuum mechanics and the ordinary state-based PD for the linear momentum balance is shown. The main difference

from a mathematical point of view is that the PD theory is an integral formulation whereas the continuum mechanical theory is a partial differential equation. Therefore, if the material is discontinuous the continuum mechanics must fail. If the integral domain is zero PD and CM will be equal, see Equation 1.

Multiple PD formulations exist. The simplest, the bond based (BB) formulation, was presented in 2000 [4]. Therein, materials are limited to a Poisson ratio of $\frac{1}{4}$ for 3D and 2D plane strain problems as well es $\frac{1}{3}$ for 2D plane stress problems [36]. To overcome these restrictions, enhancements of the method have been developed. The so called ordinary (OSB) and non-ordinary state-based (NOSB) formulation of PD are the result.

2.1 Ordinary state-based peridynamics

In the original BB formulations, bond forces only depend on a single pair of material points. The state-based formulation considers bond forces dependent of deformations of all neighboring material points. The state-based PD is able to describe materials loosen the requirements on the Poisson ratio. It must be noted that, within the state-based peridynamic framework, there is no notion of connectivity such as a spring like force between two neighboring material points. There simply is a potential between them. The equation of motion of the OSB-PD is represented as

$$\rho\left(\mathbf{x}\right)\ddot{\mathbf{u}}\left(\mathbf{x},t\right)=\int_{\mathcal{H}}\left(\underline{\mathbf{T}}[\mathbf{x},t]\langle\mathbf{x}^{'}-\mathbf{x}\rangle-\underline{\mathbf{T}}[\mathbf{x}^{'},t]\langle\mathbf{x}-\mathbf{x}^{'}\rangle\right)dV+\mathbf{b}\left(\mathbf{x},t\right) \tag{1}$$

where $\mathcal{H}$ is a spherical neighborhood of radius or horizon δ centred at $\mathbf{x}$ and where $\underline{\mathbf{T}}$ is the force vector state field. All points x' within the horizon of x are called family of x. It maps the force of the bond $\langle\mathbf{x}^{'}-\mathbf{x}\rangle$ to force densities per volume [37]. The variables $\mathbf{b}$, ρ, $\mathbf{u}$ and $\ddot{\mathbf{u}}$ are the external forces, the mass density, the displacement and the acceleration.

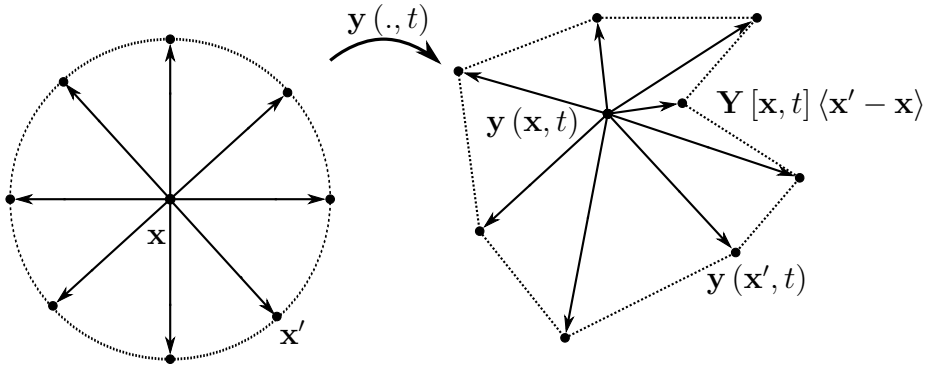

Figure 3: Family: initial & deformed configuration with deformation state $\underline{\mathbf{Y}}$ [35]

$\underline{\mathbf{T}}$ has to ensure the consistency with basic physical principles as the balance of linear momentum. This can be shown for any $\underline{\mathbf{T}}$. To describe a material, constitutive models are needed. These models map specific deformation vector state fields $\underline{\mathbf{Y}}$ in the force vector state $\underline{\mathbf{T}}$.

$$\lim_{\mathcal{H}\to 0}\int_{\mathcal{H}}\left(\underline{\mathbf{T}}[\mathbf{x},t]\langle\mathbf{x}^{'}-\mathbf{x}\rangle-\underline{\mathbf{T}}[\mathbf{x}^{'},t]\langle\mathbf{x}-\mathbf{x}^{'}\rangle\right)dV=\text{div}(\boldsymbol{\sigma}) \tag{2}$$

2.2 Material model

It is assumed that the elastic strain energy in a PD solid is equal to the energy of the CM model. In that case, it is supposed that there is a PD strain energy density function $W(\Delta)$: $V\to\Re$ such, that for some choice of the deformation gradient

$$\underline{\mathbf{Y}}(\boldsymbol{\xi})=\mathbf{F}\boldsymbol{\xi}=\mathbf{F}\langle\mathbf{x}'-\mathbf{x}\rangle\quad\forall\boldsymbol{\xi}\in\mathcal{H}. \tag{3}$$

Then the PD constitutive model corresponds to the classical constitutive model at $\mathbf{F}$ [37, 38]. With the extension scalar state $\underline{e}$

$$\underline{e}=\underline{y}-\underline{x},\qquad\underline{y}=|\underline{\mathbf{Y}}|,\qquad\underline{x}=|\underline{\mathbf{X}}| \tag{4}$$

the pairwise force density for an isotropic elastic PD solid

$$\underline{t}=\frac{3K\theta}{V_w}\underline{\omega x}+\frac{15G}{V_w}\underline{\omega e}^{d} \tag{5}$$

can be determined utilizing the bulk modulus K and the shear modulus G. The variables θ and the deviatoric part of the extension scalar state $\underline{e}^{d}$ are given as

$$\theta=\frac{3}{V_w}\int_{\mathcal{H}}(\underline{\omega x})\cdot\underline{e}dV\quad\text{and}\quad\underline{e}^{d}=\underline{e}-\frac{\theta\underline{x}}{3}\quad. \tag{6}$$

The value V_w is the weighted volume and $\underline{\omega}$ is the influence function which can be used to weight the bond stiffness related to the position in $\mathcal{H}$. It is a part of the constitutive response. The complete derivation is given in [37]. The model is similar to the classical one

$$\boldsymbol{\sigma}=K\mathbf{I}\text{tr}(\boldsymbol{\epsilon})+2G\boldsymbol{\epsilon}^{d}, \tag{7}$$

where $\boldsymbol{\sigma}$ is the mechanical stress, $\text{tr}(\boldsymbol{\epsilon})$ is the trace of the mechanical strain and $\boldsymbol{\epsilon}^{d}$ is the deviatoric part of the mechanical strain.

2.3 Damage model

One method of introducing failure into PD is through the irreversible breaking of "bonds" by setting the potential between them to zero. Failure is introduced by allowing the removal of this potential when certain physical variables reach a critical level [39].

$$w_c=\frac{4G_0}{\pi\delta^4} \tag{8}$$

The critical micro potential can be determined using the energy release rate G_0 in Equation 8. [16, 39] describe an energy-based failure criterion which is valid for state-based analysis

by comparison of the critical energy density to the energy density of each state between material points. If the bonds micro potential is greater than this value the bond is deleted. With the history-dependent scalar valued function $\chi(\boldsymbol{\xi}, t)$

$$\chi(\underline{\boldsymbol{e}}\langle\boldsymbol{\xi}\rangle, t) = \begin{cases} 1 & \text{if } w(\underline{e}\langle\boldsymbol{\xi}\rangle) < w_c \text{ for all } 0 < t' < t \\ 0 & \text{otherwise} \end{cases} , \tag{9}$$

the damage model can be included in Equation 5.

$$\underline{t} = \chi(\underline{\boldsymbol{e}}\langle\boldsymbol{\xi}, t) \left(\frac{3K\theta}{V_w} \underline{\omega x} + \frac{15G}{V_w} \underline{\omega e}^d \right) \tag{10}$$

Each "bond" has a simple damage law as shown in Figure 4a, whereas the resulting integral material response is illustrated in Figure 4b. It can be seen that the integral behavior corresponds to a standard analytical traction-separation law [3]. The dissipated energy in the material is simply the integral of the bond breakage energies over all the broken bonds in the family [40].

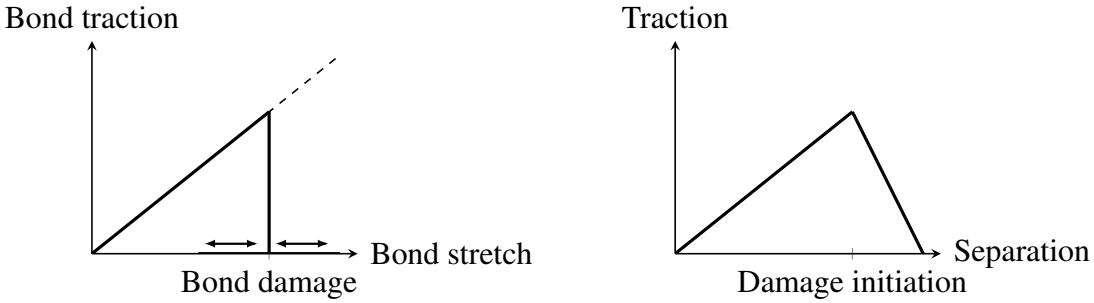

(a) Local behavior of one bond (b) Integral response of the material [3]

Figure 4: Comparison of the bond and integral material damage response

The damage law used in this publication is much simpler. It is assumed that for the one-dimensional cases considered, a critical bond elongation determined in CM can be used as input for the so-called critical stretch criterion, as done by [41] for bond-based peridynamics. In that case Equation 9 is reformulated to

$$\chi(\underline{\boldsymbol{e}}\langle\boldsymbol{\xi}\rangle, t) = \begin{cases} 1 & \text{if } \frac{\mathbf{y}(\mathbf{x}',t)-\mathbf{y}(\mathbf{x},t)}{|\mathbf{x}'-\mathbf{x}|} < \epsilon_{crit} \text{ for all } 0 < t' < t \\ 0 & \text{otherwise} \end{cases} \tag{11}$$

with ϵ_c as critical stretch value. [3] point out that this method is derived from BB-PD and that the concept may not apply in state-based material models as used in the current study. However, no other failure model has been implemented in the current numerical framework yet.

3. PROBLEM

In a first step, the behavior of the fibre-embedding epoxy matrix is investigated. Matrix cracking is a dominating mechanism for the failure behavior of the overall FRP material and

is most likely to cause other phenomena in the course of damage evolution [2]. Therefore, tensile material tests are performed and evaluated on bulk LY564 epoxy resin tensile specimen, as shown in Figure 5. The goal is to describe the individual component material properties and failure patterns before application in a more complex structure as shown in Figure 1b.

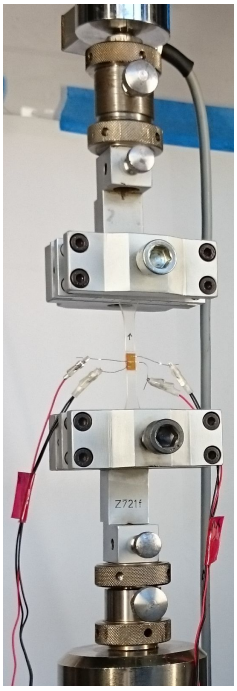

(a) Static test rig

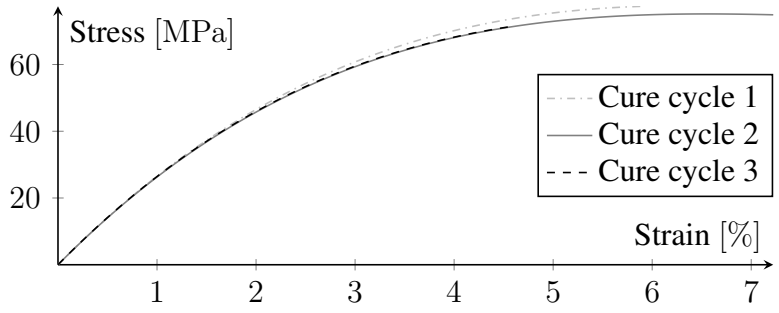

(b) Effective LY564 stress-strain curve

(c) Fracture plane micrograph

Figure 5: Bulk resin tensile test

3.1 Specimen geometry

The tested structure is a bulk resin test specimen according to DIN EN ISO 527-2 with geometry 1BA. The specimen geometry and its dimensions are shown in Figure 6 and Table 1.

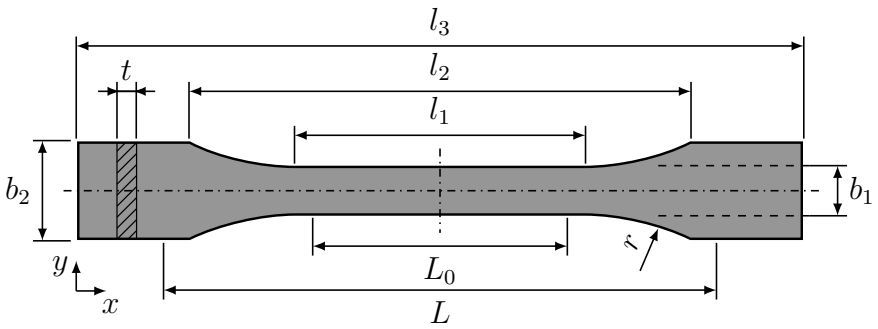

Figure 6: Bulk tension test dimensions [DIN EN ISO 527-2, 2012]

	Variable & Description	Unit	Standard	Model & Test
l_3	Overall length	mm	≥ 75	75
l_1	Parallel narrow length	mm	30.0 ± 0.5	30
r	Radius	mm	≥ 30	40.45
l_2	Distance between wide parallel edges	mm	58 ± 2	58
b_2	Wide parallel edge width	mm	10.0 ± 0.5	10
b_1	Narrow parallel edge width	mm	5.0 ± 0.5	5
t	Preferred thickness	mm	≥ 2	2
L_0	Measuring length	mm	25.0 ± 0.5	25
L	Clamp distance	mm	${l_2}^{+2}_{0}$	58

Table 1: Bulk tensile dimensions for test specimen 1BA [DIN EN ISO 527-2, 2012]

The load-displacement curves are measured using strain gauges on one side of the specimen. The resulting unsymmetrical behavior in the area of the strain gauge in combination with the localised change in stiffness in this area leads to failure in the area of the strain gauge.

3.2 Material properties

Low viscosity epoxy resin Araldite LY 564 with Aradur 22962 hardener from Huntsman [42] is used. The material properties can be found in Table 2.

Variable & Description		Unit	[42]	Test	Literature	Model
ρ	Density	$1 \cdot 10^{-9}\,\mathrm{t\,mm^{-3}}$	$1.1 - 1.2$	-	-	1.15
E	Tensile modulus	$\mathrm{N\,mm^{-2}}$	$2800 - 3300$	3190	-	3190
ν	Poisson ratio	-	-	0.334	-	0.334
ε_u	Failure strain	%	$3.5 - 8.0$	7.2	-	7.2
G_{IC}	Fracture energy	$\mathrm{N\,mm^{-1}}$	$0.2 - 0.26$	-	[43] 0.2	0.2

Table 2: Araldite LY 564/Aradur 22962 material properties

In order not to complicate the work in the present study, only linear material response and brittle fracture is considered. The material in the peridynamic simulation with Peridigm is performed using the linear peridynamic solid (LPS) material model. It has to be noted that the respective material model does not offer surface correction.

4. IMPLEMENTATION

4.1 Computational framework

Peridigm is used in the context of the present study [44]. It is an open-source computational state-based PD code developed at Sandia National Laboratories for massively-parallel multi-physics simulations. Peridigm uses a FE mesh as basis for its discretizations. Hexahedron and tetrahedron elements are transformed into peridynamic collocation points and associated with the respective element volume. Different material properties can be assigned by dividing the model into multiple blocks.

4.2 Stochastic model

To reduce possible dependencies of the solution from the underlying discretization scheme, a stochastic distribution of elastic material properties is proposed to incorporate the statistical nature of damage initiation (Figure 7). Additionally, this gives a possibility to check whether a failure pattern is driven by the chosen discretization or an actual phenomenon. [45] published a similar idea for capturing damage evolution by introducing fluctuations in the critical stretch by means of a Weibull or other distribution. The stochastic distribution of the elastic constants is also motivated by scatter in stress-strain curves and locations of failure of different test specimen and findings in micrographs in the bulk resin specimen (Figure 5). These deviations may be caused by micro-voids, locally varying degree of cure in the epoxy material or slight disparities of the specimen geometries caused by the machining process. Introduction of a stochastic material distribution has the goal to filter and numerical effects in the simulation and to ensure, that the dominating effect causing the physical failure is adequately described in the numerical model. The calculations have to be performed multiple times with different stochastic distributions to assure the dominating effect is adequately triggered.

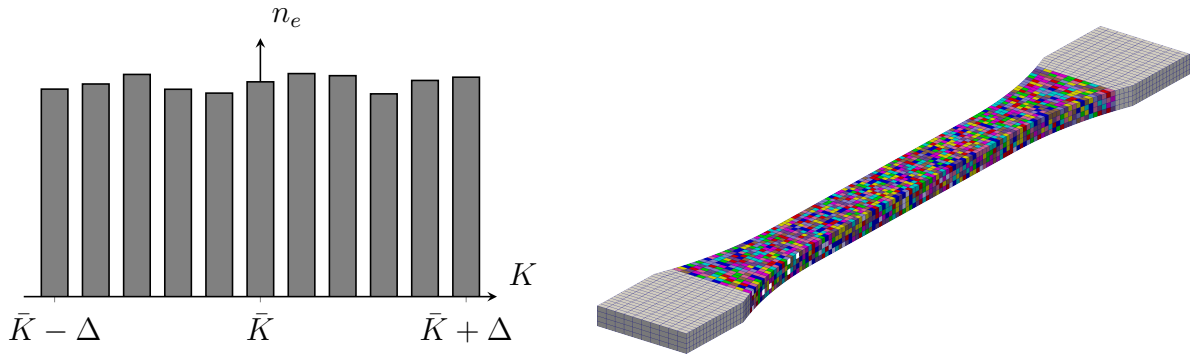

(a) Simple stochastic model (b) Base FE mesh with stochastic block distribution

Figure 7: Implementation of stochastic material distribution for PD simulations

When Peridigm computes the internal force, it computes a force state at each node in the model and applies that force state to each bond that is attached to the node. For each bond,

the resulting force density is applied to the node itself, and negative one times the force density is applied to the node on the other end of the bond. This is consistent with the state-based formulation in Equation 1. The way Peridigm handles material interfaces is basically a direct application of Equation 1. The result at a material interface is an average of the two material models. Thus, a block-based stochastic model is possible by simply assigning materials with different elastic constants.

As the nature of the distribution of stochastic effects in the real specimen is currently unknown, a rather simple approach is chosen for their modeling. During the creation of the specimen, elements in the damage-prone area are stochastically associated to multiple block definitions. Each block is associated with a material that has a defined deviation from the nominal elastic constants. The number of different block definitions and the maximum deviation from the nominal elastic constants can be chosen randomly. More complex distribution, such as Gaussian or Weibull distribution, may be implemented in the future if the approach seems promising.

5. MODEL

5.1 Discretization

A FE based mesh input is used by Peridigm. As it is expected there are differences in the choice of the horizon and element size for structured and unstructured based meshes, both are considered here. The specimen creation in a versatile parametric model generator allows for a quick change of the underlying discretization scheme and the element size. The base FE models and resulting PD discretizations are shown in Figure 8.

The structured mesh is doubly symmetric regarding the specimen x-y- as well as the x-z-plane. The unstructured meshes are only symmetric about the x-z-plane.

Especially in higher dimensions, the horizon cannot be too large either as this results in the boundary layer, where displacement boundary conditions are imposed, being the majority of the simulation domain [28]. Thus, a no-damage zone (red) is introduced in the vicinity of the specimen ends. In this region failure is not modeled to avoid effects of the boundary conditions on the failure behavior. Based on the findings in the experiments this approach is valid.

5.2 Loads and boundary conditions

Both specimen ends are clamped in the test fixture. The tensile experiments are strain-controlled by means of a constant velocity on one of the clamping regions. The homogeneous displacement and inhomogeneous velocity boundary conditions are applied on respective node sets at the specimen ends. As these sets are defined on the base FE mesh, there is a small deviation of the application region in the PD model. This has no effect on the results. Various combinations of displacement boundary conditions were investigated. The influence on the results is negligible.

Madenci and Oterkus [46] point out, that simply imposing constant boundary condition

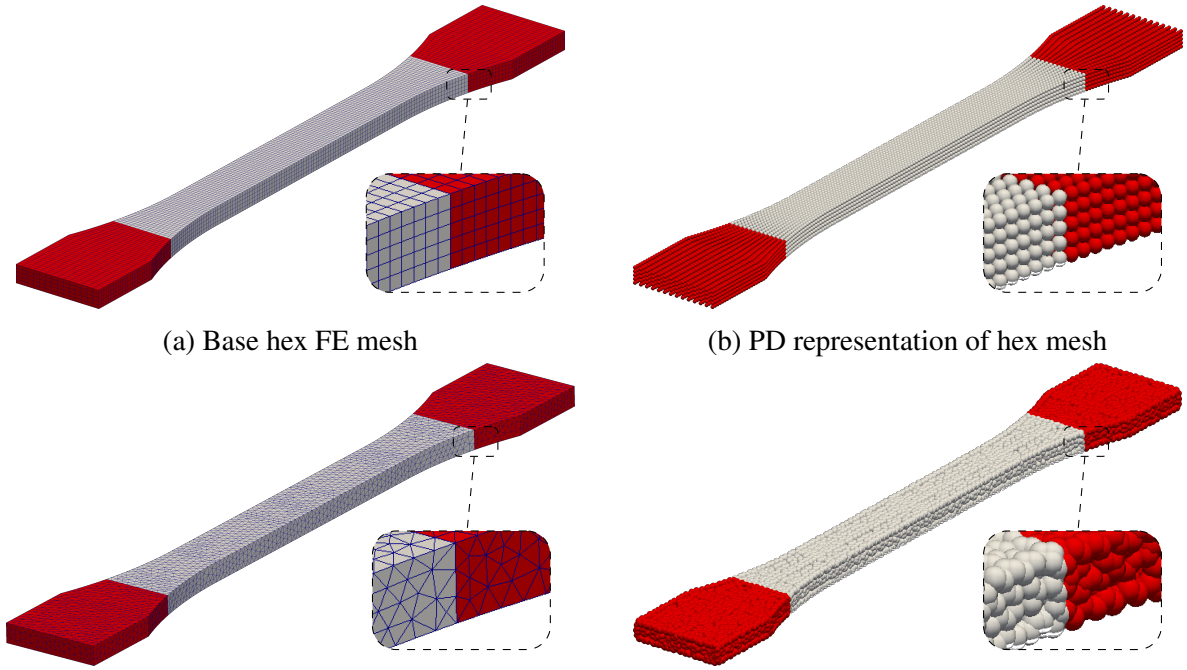

(a) Base hex FE mesh

(b) PD representation of hex mesh

(c) Base tet FE mesh

(d) PD representation of tet mesh

Figure 8: Discretization schemes and PD representation

values on a material regions leads to incorrect behavior of the actual boundary and the domain within a distance of one horizon from the application region. A modified approach to reflect the correct boundary conditions is proposed but not used here as the no-failure-zone in the model is large enough to smooth boundary effects.

6. RESULTS

6.1 Convergence

In a first step extensive convergence studies are carried out. Therefore, only the elastic part of the material behavior is considered. The load-displacement curves of the PD simulations are compared to the solution obtained by the implicit nonlinear solution in the commercial finite element solver Abaqus. Identical meshes are used in both cases. Using the versatile parametric model generator, the identical discretizations are written for Peridigm and Abaqus.

The stiffness convergence is evaluated by means of the load-displacement behavior. Two aspects of convergence are considered. At first it is investigated if the load-displacement curves asymptotically approach a common course. On the other hand, the load-displacement curve from the local FE solution obtained with Abaqus is used as a second convergence criterion for this simple one-dimensional loading condition. It is not expected that the PD solution must necessarily exactly coincide with the FE result. But for this simple test, large deviations should also not occur in the elastic regime of the material response.

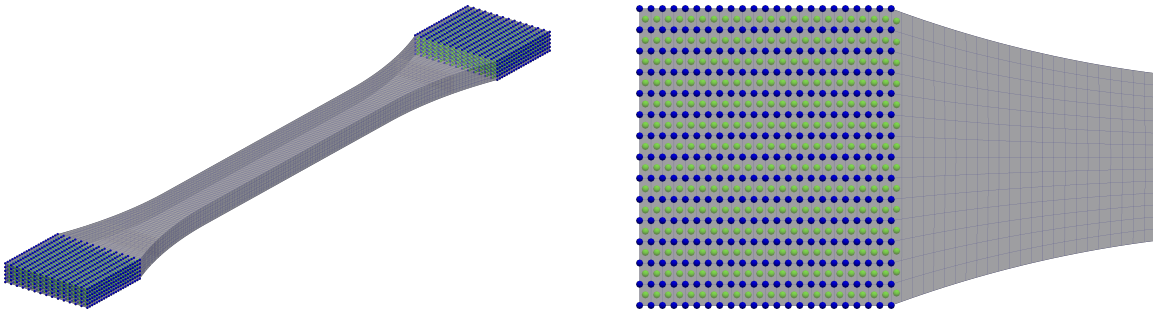

(a) Iso view (b) Detail of FE (blue) and PD (green) node set

Figure 9: Constraint and load introduction domains

6.1.1 Hex mesh

Stiffness Figure 10 shows the respective results for an element edge length dx of $0.4\,\mathrm{mm}$ and a structured mesh for different horizons. This element edge length is defined over the thickness of the specimen. Due to the dimensions from Table 1, the in-plane element edge length is $0.395\,\mathrm{mm}$ in x- and $0.357\,\mathrm{mm}$ in y-direction. In this study, the horizon is specified by means of an absolute value as proposed by [14, 15] to be able to directly compare the behavior between different element edge length. The non-continuous curves for the PD results are caused by small oscillation in the explicit solution in Peridigm without any damping and a small number of output time steps.

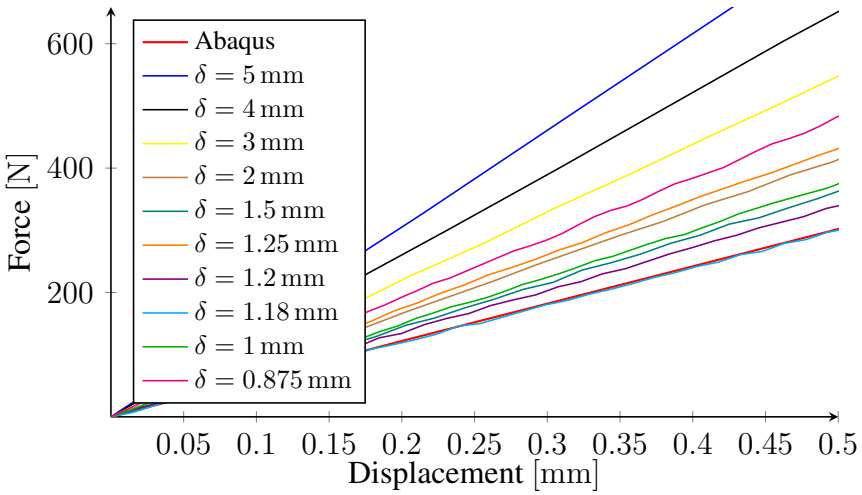

Figure 10: Force-displacement plot in elastic region for hex-mesh with $dx = 0.4\,\mathrm{mm}$ and various horizons

For the chosen element edge length of $dx = 0.4\,\mathrm{mm}$, the stiffness reduces with decreasing horizon. This finding does not correspond to the results in [47] where a LPS material model

produces a less stiff behavior than expected. The decrease in stiffness is obtained until $m \approx 3$, here $m = 2.95$ for a horizon of $\delta = 1.18\,\mathrm{mm}$. This matches $m_z = 2.95$, $m_y = 3.31$ and $m_x = 2.99$. The converged PD solution matches the FE solution. If the horizon is decreased below this value, the stiffness rises again compared to the FE solution. This may be caused by the fact, that not enough neighboring points interact in the horizon of a single point to depict the correct material behavior in all directions, including transversal contraction.

For element edge length above $0.4\,\mathrm{mm}$ and thus five PD collocation points over the specimen thickness, a similar behavior exists with the exception that the local FE solution is never reached. This seems to be the result of the missing surface correction in the chosen LPS material model implementation in Peridigm. For element sizes smaller than $0.4\,\mathrm{mm}$ and thus more elements over the specimen thickness a horizon with good agreement can be found for all considered cases.

The results of the study for different element sizes is shown in Figure 11. Since it is impossible to show the load-displacement curves for all combinations in the context of this study, only the relative error of the force at a displacement of $0.1\,\mathrm{mm}$ in the load introduction region to the FE solution with an element edge length of $0.2\,\mathrm{mm}$ is compared. Results in the upper left corner of the figure are not available as the horizon would be smaller than the element size. The smaller the failure of a combination is, the brighter a point is. A white point corresponds to an error of zero. The minimum combination of each element size and horizon is shown by dashed lines.

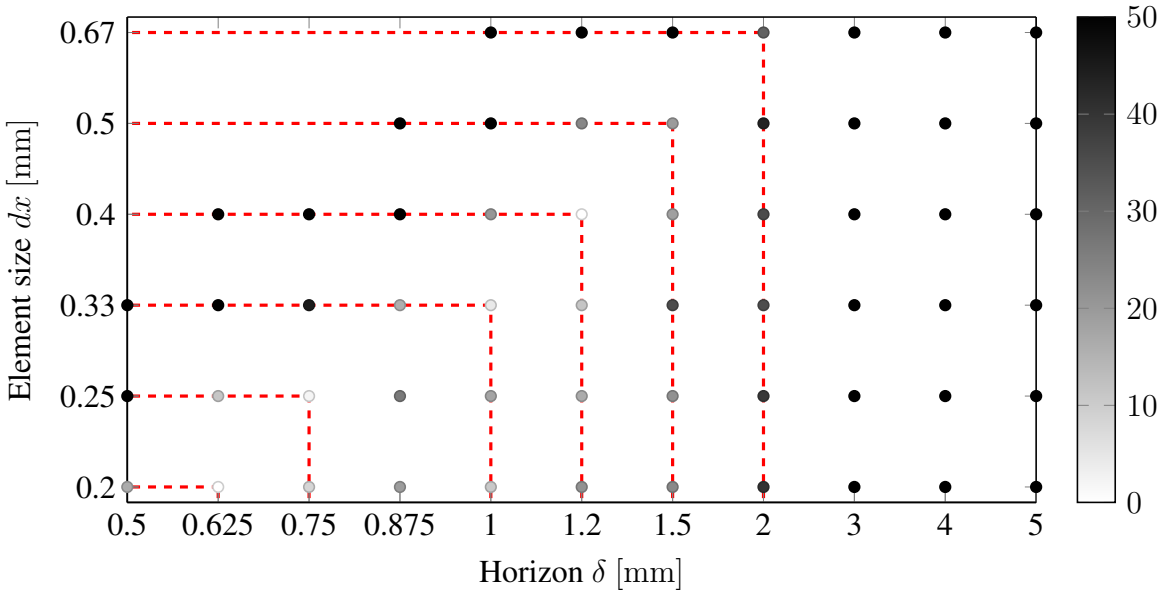

Figure 11: Relative force error [%] to FEM solution for hex-mesh

It can be seen, that the convergence behavior is neither smooth nor continuous. For all considered combinations a value of $m \approx 3$ leads to the minimum error compared to the elastic FE response. Also, the error is reduced for finer discretizations. If the mesh is too coarse or the

horizon too high, large deviations occur. Here, the limit is that the multitude of peridynamic families should experience no effect of surface correction. This is not assured for $\delta \geq 1\,\mathrm{mm}$ for the current model thickness as the characteristic length dimension. As expected, the smallest error is achieved for the finest discretization (Figure 12). However, the error for $dx = 0.4\,\mathrm{mm}$ is sufficiently small and this element size allows a suitable calculation time for the following studies.

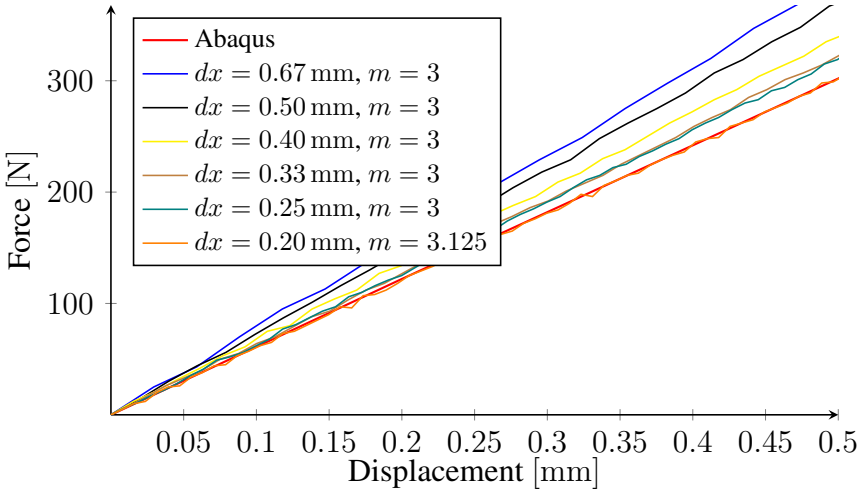

Figure 12: Force-displacement plot in elastic region for hex-mesh with $m \approx 3$

Failure According to [48], the choice of the horizon is constrained by a relationship between critical stretch and strain energy release rate. For bond-based peridynamics the respective equation is also given in [3, 17]. It must be noted that the equation is based on the Griffith crack model which require an existing pre-crack which is not present in the current model. [49] claims that a similar equation for state-based model exists. However, the derivation is presumably based on assumptions valid for BB-PD.

$$\epsilon_{c.BB} = \sqrt{\frac{5G_c}{9K\delta}} \qquad \epsilon_{c.SB^*} = \sqrt{\frac{G_c}{\left[3G + \left(\frac{3}{4}\right)^4 \left(K - \frac{5G}{3}\right)\right]\delta}} \tag{12}$$

For both equations, $\epsilon_c = f(\delta^{-\frac{1}{2}})$. If a critical stretch is chosen for a specific horizon, the critical stretch can be recalculated for any other horizon value by means of this relationship. If the results are compared, for a 1D case, failure should occur at the same displacement. To check this assumption, the load displacement curves for $dx = 0.4\,\mathrm{mm}$ are compared until failure for different horizons (Figure 13).

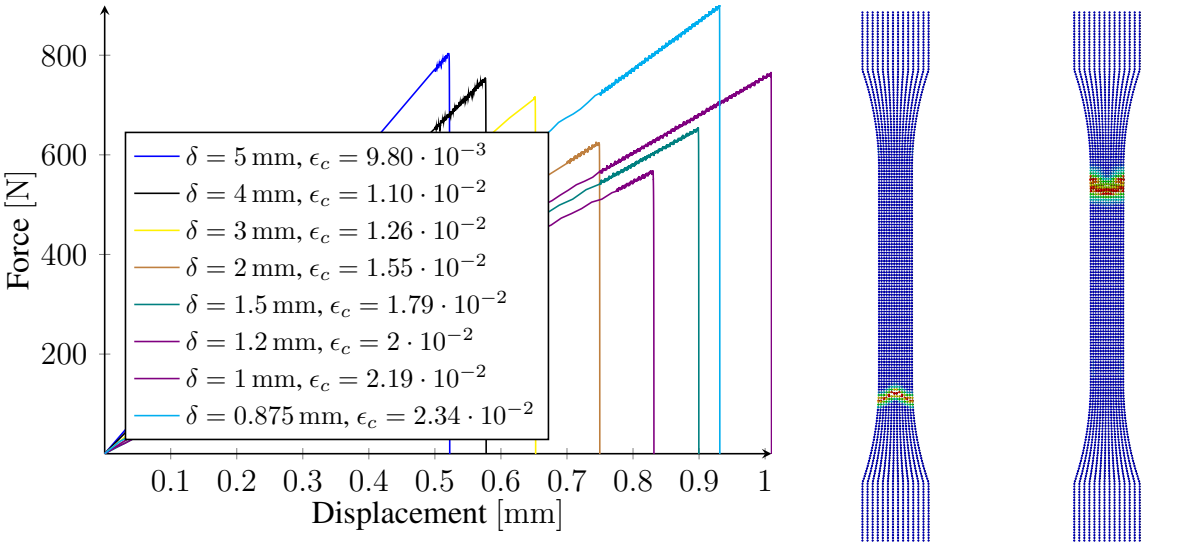

(a) Force-displacement plot until failure (b) $\delta = 1.2\,\mathrm{mm}$ (c) $\delta = 2\,\mathrm{mm}$

Figure 13: Failure for hex-mesh with $dx = 0.4\,\mathrm{mm}$ and various horizons

It can be seen, that Equation 12 does not hold for state-based PD. The specimen fail at totally different displacements. A similar pattern as for the stiffness convergence can be seen. This may be caused by the unequal force states of two points in a "bond". However, the failure behavior might be strongly influenced by the missing surface correction in the LPS material model used in Peridigm. The only proper way to calibrate failure currently is to set the critical stretch to a value where the specimen fails at the same displacement as in the FE simulation or enhance Peridigm by an energy based failure criterion.

In quasi-static loading a symmetrical failure pattern is expected at 4 locations of the specimen. However, a fairly high velocity is chosen to keep calculation times on a manageable level. Due to the combination of explicit time integration without any damping and this velocity it may be possible that inertia effects have an influence on the location of failure. In that case the specimen should fail in the top half, the side with the velocity constraint. The expected location of failure is not achieved for the converged horizon but for the higher one. However, it is possible that the loading speed is small enough that the damage location is dominated by small numerical effects.

Due to the specimen symmetry failure occurs symmetrically on both sides and evolves in the direction of the specimen mid-plane. The location of failure is comprehensible and lies in the transition to the radius. Mild notch effects due to the change in stiffness and long-range effects of the boundary conditions cause this behavior. A slight kink develops in the crack path, which is most likely to be caused by the discretization pattern and the non-constant PD point volume in the mesh transition domain.

For a 1D stress-state in a BB-PD code [41] proposed that the critical stretch can be taken equal to the maximum principal strain from CM. From a comparison to the Abaqus XFEM

solution one can see that this assumption is not valid in the current context. The displacement at failure is even highly unequal between the two discretization types for each converged solution and the same critical stretch.

6.1.2 Tet mesh

Stiffness Similar studies are carried out for a FE base mesh consisting of tetrahedron elements. The results for the same element edge length are not directly comparable between structured and unstructured meshes as the latter consists of a lot more elements for the same edge length. The results of the stiffness convergence behavior are shown in Figure 14.

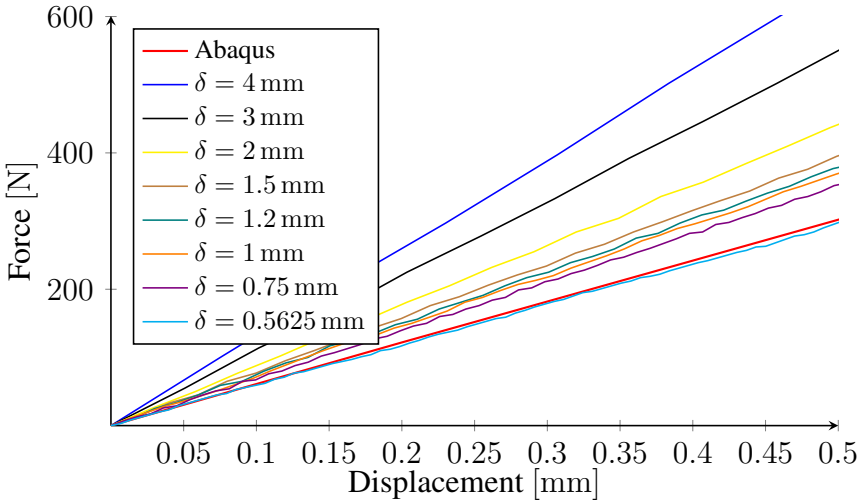

Figure 14: Force-displacement plot in elastic region for tet-mesh with $dx = 0.5\,\mathrm{mm}$ and various horizons

The stiffness decreases monotonically until the horizon is only slightly larger than one. It can therefore be said, that the unstructured discretization converges to the local FE solution for smaller horizons. The results of all combinations of element size and horizon are shown in Figure 15 with the same approach as in Figure 11.

However, this result might not reqpresent the globally converged solution. For smaller element sizes it can be observed that the stiffness decreases even below the FEM solution. If the mesh size is further decreased, the stiffness rises to the CM solution again. Unfortunately, using these small element sizes comes with tremendous expenses with respect to the calculation time and computational requirements.

Convergence is more continuous than for the hex mesh but still far from smooth over different element sizes. The minimum error occurs for a horizon slightly smaller than the element size, here a factor of $m = 1.125$.

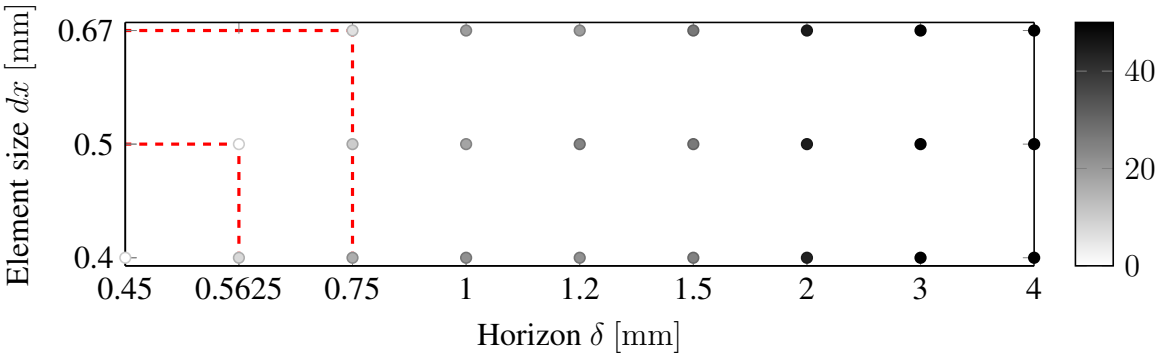

Figure 15: Relative force error [%] to FEM solution in elastic region for tet-mesh at displacement $0.1\,\mathrm{mm}$

Failure The results of the force-displacement plots with different horizons and adjusted critical stretch values are shown in Figure 16. The same observation as for the hex mesh can be made. The relationship for the critical stretch from the bond-based PD, Equation 12, does not apply for state-based PD in Peridigm.

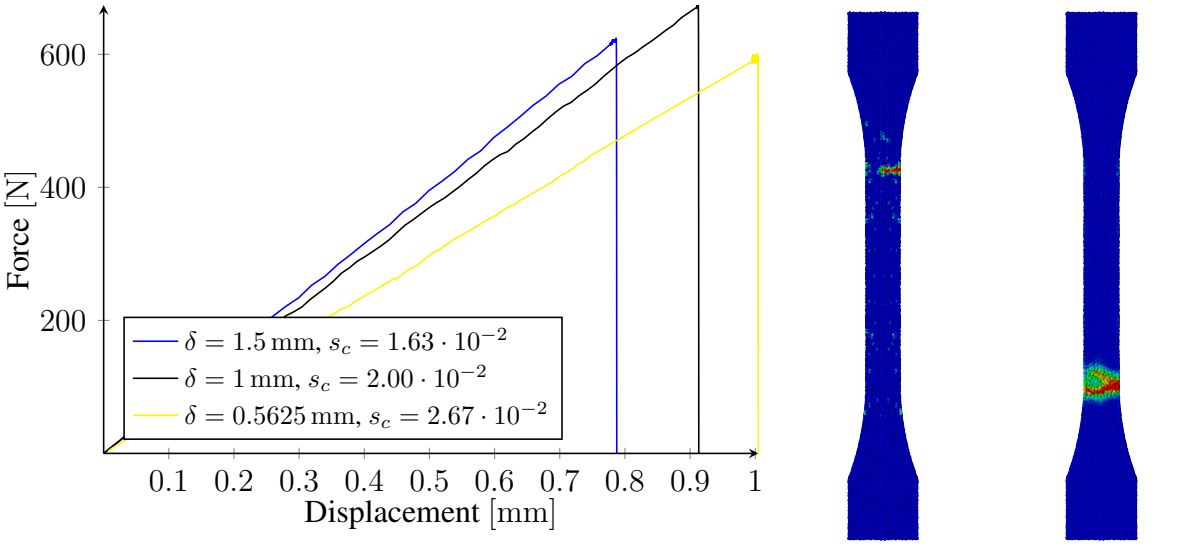

(a) Force-displacement plot until failure (b) $\delta = 0.56\,\mathrm{mm}$ (c) $\delta = 1.5\,\mathrm{mm}$

Figure 16: Failure for tet-mesh with $dx = 0.5\,\mathrm{mm}$ and various horizons

The vertical location of failure is at the expected side of the specimen for the converged horizon value. As for the hex-mesh, a higher value of the horizon leads to a more extensive failure domain. It has to be noted that in the converged solution, failure occurs at the exact location of transition in the specimen radius. In this localised area the discretization is strongly influenced by the chosen geometrical model. In the present case a subdivision of individual volumes is located there. This seems to influence the failure behavior which is comprehensible

for this quasi discrete local model. It seems a quasi continuum nonlocal approach using an unstructured mesh is well suited to capture failure mechanisms.

6.1.3 Comparison

For both discretizations at least five elements over the smallest specimen dimension should be used to be able to achieve a convergent solution with negligible errors to the continuum mechanics solution in the elastic regime. The more entropic discretization using a tet mesh and avoiding symmetries in the model leads to a more physical representation of failure. Thus, for more complex studies, the use of an unstructured mesh is proposed.

[11] found that classical elasticity theory is a subset of peridynamics and that PD converges to classical elasticity theory for small horizons. In the present study, and therefore for the numerical implementation of PD, it was found that minimizing the horizon to a bare minimum of $m = 1$ only leads to the results of the local finite element method for the unstructured discretization. Structured grids need larger horizon values of $m \approx 3$ to assure that enough family members exist so that all directions are adequately covered.

[11] also mentioned that if the only requirement for a peridynamic constitutive model is to reproduce the bulk properties, then horizon is essentially arbitrary. We found that statement to be incomplete as the material behavior is a function of the combination of discretization size and horizon if the behavior is not dominated by small-scale effects.

6.2 Stochastics

The lack of a generally valid failure criterion in state-based PD makes an assessment of the initial idea to use a stochastic material distribution for the assessment of failure initiation difficult. However, stochastics may be used to achieve the same entropy in structured discretization as in unstructured base meshes and to individualize failure locations. The comparison of the original hex model with $dx = 0.4\,\mathrm{mm}$ and horizon $\delta = 1.2\,\mathrm{mm}$ and three models with stochastic material distribution is shown in Figure 17. Ten different blocks are created with a deviation of the $2\,\%$ of the material bulk and shear modulus.

It can be seen that the overall stiffness and failure behavior does not change significantly. However, the stochastic material distribution makes it possible to spot several possible individual failure locations. One would expect a less slanted crack propagation. This can be achieved by using a finer discretization. However, a slightly angular failure path can also be observed in tests with a little different specimen geometry of the same material, see Figure 18. A contact-free displacement measurement using a video extensometer is used to avoid an influence on the crack path.

The same principal results are valid for tet meshes as shown in Figure 19 with a modulus range of $5\,\%$ around the nominal value. It can be noted that the location of failure shifts slightly away from the geometric feature bordering the two separate volumes in this region. In one case failure occurs slightly earlier as a result of the stochastic material distribution. Overall, due to the higher mesh entropy, the effect of stochastic material distribution in tet meshes is smaller

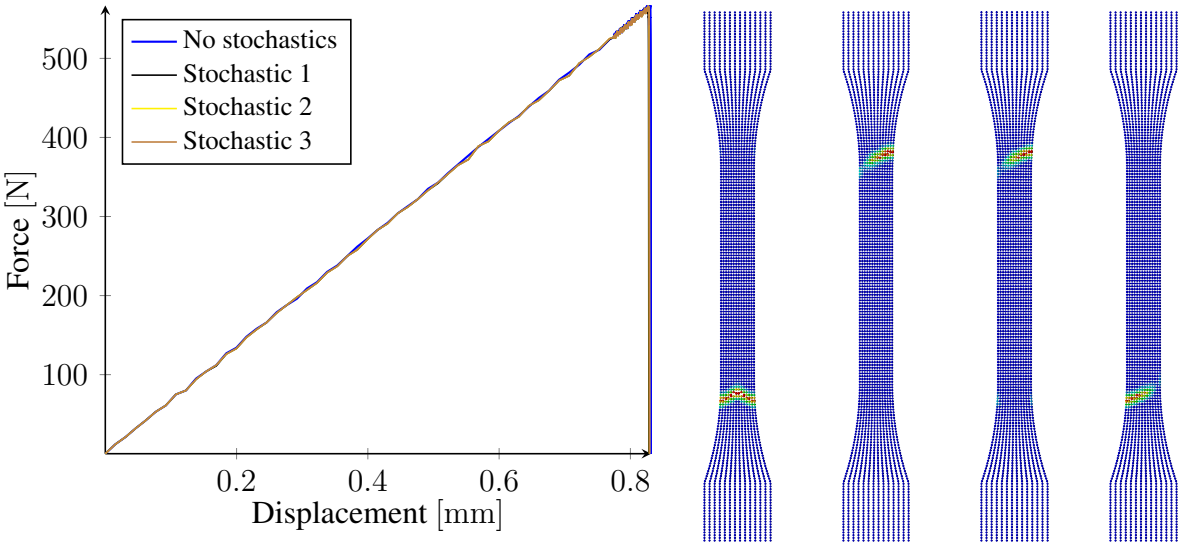

(a) Force-displacement plot until failure (b) No (c) 1 (d) 2 (e) 3

Figure 17: Failure for hex-mesh with $dx = 0.4\,\mathrm{mm}$ and stochastics

Figure 18: Angled crack path in same material specimen with different geometry [2]

than in hex meshes.

7. CONCLUSIONS

In the current study, the convergence behavior of peridynamic simulations is investigated using the open-source PD code Peridigm. Multiple base discretization schemes are compared. Different convergence behavior is observed for base hex and tet meshes. While $m \approx 3$ delivers the best results for hex meshes, $m \approx 1$ can be chosen for tet discretizations in case long-range forces have no effect and PD is merely used to improve the simulation of failure compared to CM models.

The use of stochastic material distributions in PD simulations in Peridigm is possible and gives meaningful results. It has proven to be a way to check if the results obtained in PD simulations concerning failure are dominated by numerics and discretization effects or are really the dominating physical effect.

If PD is simply used to model fracture in specimen and conditions not dominated by long-range force effects, the use of tetrahedron base meshes is recommended. The horizon can then be chosen only slightly larger than the element size. Symmetry planes in the model should be avoided. In case a hexahedron mesh is used as an input, a stochastic material distribution is a possibility to increase the model entropy and to get a more consistent prediction of the

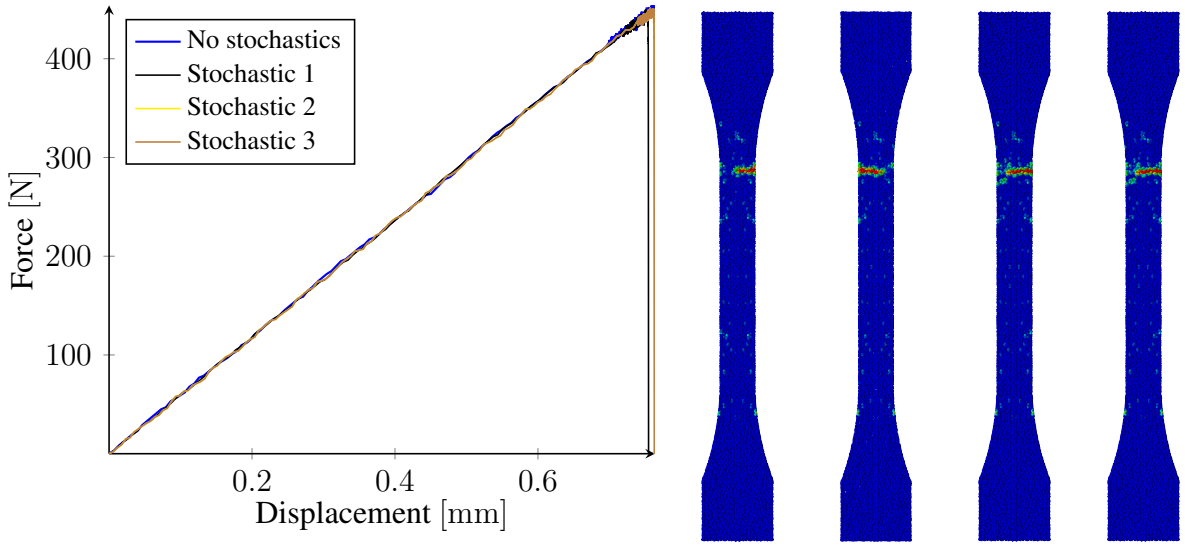

(a) Force-displacement plot until failure (b) No (c) 1 (d) 2 (e) 3

Figure 19: Failure for hex-mesh with $dx = 0.4\,\mathrm{mm}$ and stochastics

dominating failure pattern.

The critical stretch damage model must be adjusted to the discretization. The bond-based relationships to the critical strain energy release rate prove unsuited for state-based models. Thus, an energy-based failure criterion will be implemented during the next development steps.

References

[1] E.K Gamstedt and B.A Sjögren. "Micromechanisms in tension-compression fatigue of composite laminates containing transverse plies". In: *Composites Science and Technology* 59.2 (1999), pp. 167–178. DOI: http://dx.doi.org/10.1016/S0266-3538(98)00061-X.

[2] Daniel Krause. "Micromechanics of the fatigue behaviour of polymers". DLR Report 2016-26. PhD Thesis. Technical University Braunschweig, 2016.

[3] Florin Bobaru et al. *Handbook of Peridynamic Modeling*. Advances in Applied Mathematics. CRC Press, 2016.

[4] Stewart A. Silling. "Reformulation of elasticity theory for discontinuities and long-range forces". In: *Journal of the Mechanics and Physics of Solids* 48.1 (2000), pp. 175–209. DOI: 10.1016/S0022-5096(99)00029-0.

[5] Pablo Seleson, Qiang Du, and Michael L. Parks. "On the consistency between nearest-neighbor peridynamic discretizations and discretized classical elasticity models". In: *Computer Methods in Applied Mechanics and Engineering* 311 (2016), pp. 698–722. DOI: http://doi.org/10.1016/j.cma.2016.07.039.

[6] Florin Bobaru and Wenke Hu. "The Meaning, Selection, and Use of the Peridynamic Horizon and its Relation to Crack Branching in Brittle Materials". In: *International Journal of Fracture* 176.2 (2012), pp. 215–222. DOI: 10.1007/s10704-012-9725-z.

[7] Abigail G. Agwai. "A Peridynamic Approach for Coupled Fields". PhD Thesis. The University of Arizona, 2011.

[8] R. Maranganti and P. Sharma. "Length Scales at which Classical Elasticity Breaks Down for Various Materials". In: *Phys. Rev. Lett.* 98 (19 May 2007), pp. 195504-1–195504-4. DOI: http://dx.doi.org/10.1103/PhysRevLett.98.195504.

[9] Markus Zimmermann. "A continuum theory with long-range forces for solids". PhD Thesis. Massachusetts Institute of Technology, 2005.

[10] Etienne Emmrich and Olaf Weckner. "On the well-posedness of the linear peridynamic model and its convergence towards the Navier equation of linear elasticity". In: *Communication in Mathematical Sciences* 5.4 (2007), pp. 851–864. DOI: http://projecteuclid.org/euclid.cms/1199377554.

[11] Stewart A. Silling and R. Lehoucq. "Convergence of peridynamics to classical elastic theory". In: *Journal of Elasticity* 93 (2008), pp. 13–37. DOI: 10.1007/s10659-008-9163-3.

[12] Florin Bobaru and Monchai Duangpanya. "The peridynamic formulation for transient heat conduction". In: *International Journal of Heat and Mass Transfer* 53.19-20 (2010), pp. 4047–4059. DOI: http://dx.doi.org/10.1016/j.ijheatmasstransfer.2010.05.024.

[13] Youn Doh Ha and Florin Bobaru. "Studies of dynamic crack propagation and crack branching with peridynamics". In: *International Journal of Fracture* 162.1 (2010), pp. 229–244. DOI: 10.1007/s10704-010-9442-4.

[14] G. Sarego et al. "Linearized state-based peridynamics for 2-D problems". In: *International Journal for Numerical Methods in Engineering* 108.10 (2016), pp. 1174–1197. DOI: http://dx.doi.org/10.1002/nme.5250.

[15] Wenke Hu, Youn Doh Ha, and Florin Bobaru. "Peridynamic model for dynamic fracture in unidirectional fiber-reinforced composites". In: *Computer Methods in Applied Mechanics and Engineering* 217-220 (2012), pp. 247–261. DOI: https://doi.org/10.1016/j.cma.2012.01.016.

[16] John T. Foster, Stewart A. Silling, and Weinong Chen. "An Energy based Failure Criterion for use with Peridynamic States". In: *International Journal for Multiscale Computational Engineering* 9.6 (2011), pp. 675–688. DOI: http://dx.doi.org/10.1615/IntJMultCompEng.2011002407.

[17] Stewart A. Silling and E. Askari. "A meshfree method based on the peridynamic model of solid mechanics". In: *Computers and Structures* 83.17-18 (2005), pp. 1526–1535. DOI: 10.1016/j.compstruc.2004.11.026.

[18] Stewart A. Silling. *A Coarsening Method for Linear Peridynamics*. Sandia Report SAND2010-3303. Multiscale Science Department, Sandia National Laboratories, 2009.

[19] Patrick Diehl et al. "Bond-based peridynamics: a quantitative study of Mode I crack opening". In: *International Journal of Fracture* 201.2 (2016), pp. 157–170. DOI: http://dx.doi.org/10.1007/s10704-016-0119-5.

[20] Y. L. Hu, N. V. De Carvalho, and E. Madenci. "Peridynamic modeling of delamination growth in composite laminates". In: *Composite Structures* 132 (2015), pp. 610–620. DOI: 10.1016/j.compstruct.2015.05.079.

[21] Richard W. Macek and Stewart A. Silling. "Peridynamics via finite element analysis". In: *Finite Elements in Analysis and Design* 43.15 (2007), pp. 1169–1178. DOI: 10.1016/j.finel.2007.08.012.

[22] Andris Freimanis and Ainars Paeglitis. "Mesh Sensitivity in Peridynamic Quasi-static Simulations". In: *Procedia Engineering* 172 (2017). Modern Building Materials, Structures and Techniques, pp. 284–291. DOI: http://dx.doi.org/10.1016/j.proeng.2017.02.116.

[23] Florin Bobaru et al. "Convergence, adaptive refinement, and scaling in 1D peridynamics". In: *International Journal for Numerical Methods in Engineering* 77.6 (2009), pp. 852–877. DOI: 10.1002/nme.2439.

[24] Youn Doh Ha and Florin Bobaru. "Characteristics of dynamic brittle fracture captured with peridynamics". In: *Engineering Fracture Mechanics* 78.6 (2011), pp. 1156–1168. DOI: https://doi.org/10.1016/j.engfracmech.2010.11.020.

[25] Rami Jabakhanji and Rabi H Mohtar. "A peridynamic model of flow in porous media". In: *Advances in Water Resources* 78 (2015), pp. 22–35. DOI: http://dx.doi.org/10.1016/j.advwatres.2015.01.014.

[26] Shubhankar Roy Chowdhury et al. "A peridynamic theory for linear elastic shells". In: *International Journal of Solids and Structures* 84 (2016), pp. 110–132. DOI: http://dx.doi.org/10.1016/j.ijsolstr.2016.01.019.

[27] Ziguang Chen and Florin Bobaru. "Peridynamic modeling of pitting corrosion damage". In: *Journal of the Mechanics and Physics of Solids* 78 (2015), pp. 352–381. DOI: http://dx.doi.org/10.1016/j.jmps.2015.02.015.

[28] Pablo Seleson and David J. Littlewood. "Convergence studies in meshfree peridynamic simulations". In: *Computers & Mathematics with Applications* 71.11 (2016). Proceedings of the conference on Advances in Scientific Computing and Applied Mathematics. A special issue in honor of Max Gunzburger's 70th birthday, pp. 2432–2448. DOI: https://doi.org/10.1016/j.camwa.2015.12.021.

[29] Xiaochuan Tian and Qiand Du. "Analysis and Comparison of Different Approximations to Nonlocal Diffusion and Linear Peridynamic Equations". In: *SIAM Journal on Numerical Analysis* 51.6 (2013), pp. 3458–3482. DOI: https://doi.org/10.1137/13091631X.

[30] X. Chen and Max Gunzburger. "Continuous and discontinuous finite element methods for a peridynamics model of mechanics". In: *Computer Methods in Applied Mechanics and Engineering* 200 (2011), pp. 1237–1250. DOI: https://doi.org/10.1016/j.cma.2010.10.014.

[31] Qiang Du et al. "A posteriori error analysis of finite element method for linear nonlocal diffusion and peridynamic models". In: *Mathematics of Computation* 82 (2013), pp. 18889–1922. DOI: https://doi.org/10.1090/S0025-5718-2013-02708-1.

[32] M.S. Breitenfeld et al. "Non-ordinary state-based peridynamic analysis of stationary crack problems". In: *Computer Methods in Applied Mechanics and Engineering* 272 (2014), pp. 233–250. DOI: https://doi.org/10.1016/j.cma.2014.01.002.

[33] Etienne Emmrich and Olaf Weckner. "The peridynamic equation and its spatial discretisation". In: *Mathematical Modelling and Analysis* 12.1 (2007), pp. 17–27. DOI: http://dx.doi.org/10.3846/1392-6292.2007.12.17-27.

[34] Ziguang Chen, Drew Bakenhus, and Florin Bobaru. "A constructive peridynamic kernel for elasticity". In: *Computer Methods in Applied Mechanics and Engineering* 311 (2016), pp. 356–373. DOI: http://dx.doi.org/10.1016/j.cma.2016.08.012.

[35] Stewart A. Silling. *Linearized Theory of Peridynamic States*. Sandia Report SAND2009-2458. Multiscale Science Department, Sandia National Laboratories, 2009.

[36] Dan Huang, Guangda Lu, and Pizhong Qiao. "An improved peridynamic approach for quasi-static elastic deformation and brittle fracture analysis". In: *International Journal of Mechanical Sciences* 94-95 (2015), pp. 111–122. DOI: http://dx.doi.org/10.1016/j.ijmecsci.2015.02.018.

[37] Stewart A. Silling et al. "Peridynamic States and Constitutive Modeling". In: *Journal of Elasticity* 88 (2007), pp. 151–184. DOI: 10.1007/s10659-007-9125-1.

[38] Adair R. Aguiar and Roger Fosdick. "A constitutive model for a linearly elastic peridynamic body". In: *Mathematics and Mechanics of Solids* 19.5 (2014), pp. 502–523. DOI: 10.1177/1081286512472092.

[39] John T. Foster, Stewart A. Silling, and Wayne W. Chen. "State Based Peridynamic Modeling of Dynamic Fracture". In: *Proceedings of the SEM Annual Conference, Albuquerque, USA*. 2009, pp. 1–6.

[40] Stewart A. Silling and R. B. Lehoucq. "Peridynamic Theory of Solid Mechanics". In: *Advances in Applied Mechanics* 44 (2010), pp. 73–168. DOI: 10.1016/S0065-2156(10)44002-8.

[41] Walter Gerstle, Nicolas Sau, and Stewart Silling. “Peridynamic Modeling of Plain and Reinforced Concrete Structures”. In: *18th International Conference on Structural Mechanics in Reactor Technology (SMiRT 18), 7-12 August 2005, Beijing, China*. 2005.

[42] *Araldite® LY 564 / Aradur ® 22962 data sheet*. Huntsman International LLC. Salt Lake City, Utah, USA, June 2009.

[43] Dimitrios E. Sikoutris. “Fire Response of Composite Aerostructures”. PhD Thesis. University of Patras, 2012.

[44] Michael L. Parks et al. *Peridigm Users' Guide*. Sandia Report Tech. Report SAND2012-7800. Albuquerque, New Mexico 87185 and Livermore, California 94550, USA: Sandia National Laboratories, 2012.

[45] Stewart A. Silling, Paul Demmie, and Thomas L. Warren. *Peridynamic Simulation of High-Rate Material Failure*. 2007 ASME Applied Mechanics and Materials Conference, Austin, TX. June 2007.

[46] Erdogan Madenci and Selda Oterkus. “Ordinary state-based peridynamics for plastic deformation according to von Mises yield criteria with isotropic hardening”. In: *Journal of the Mechanics and Physics of Solids* 86 (2016), pp. 192–219. DOI: https://doi.org/10.1016/j.jmps.2015.09.016.

[47] John A. Mitchell, Stewart A. Silling, and David J. Littlewood. “A Position-Aware Linear Solid Constitutive Model for Peridynamics”. In: *Mechanics of Materials and Structures* 10.5 (2015), pp. 539–557. DOI: 10.2140/jomms.2015.10.539.

[48] ByoungSeon Jeon, Ross J. Stewart, and Izhar Z. Ahmed. “Peridynamic simulations of brittle structures with thermal residual deformation: strengthening and structural reactivity of glasses under impacts”. In: *Proceedings of the Royal Society of London A: Mathematical, Physical and Engineering Sciences* 471.2183 (2015), p. 20150231. DOI: 10.1098/rspa.2015.0231.

[49] Erdogan Madenci and Erkan Oterkus. *Peridynamic Theory and Its Applications*. Vol. 1. Springer, New York, 2014. DOI: 10.1007/978-1-4614-8465-3. eprint: arXiv:1011.1669v3.